Evidence of synergy between neoclassical and turbulent impurity transports

Y. Sarazin, D. Estève, P. Donnel, S. Breton, X. Garbet, V. Grandgirard, C. Bourdelle,
G. Dif-Pradalier, C. Ehrlacher, Ph. Ghendrih, G. Latu, C. Passeron
CEA, IRFM, F-13108 Saint-Paul-lez-Durance cedex, France.

In tokamak plasmas, the radial transport of matter and energy, governed by collisions and turbulence, is intrinsically multi scales. While neoclassical transport results from stationary large scale structures, namely static $(m,n) = (1,0)$ modes (m,n = poloidal, toroidal Fourier wave numbers), turbulence develops fluctuating small scale modes $m,n \gg 1$. On the basis of this scale separation, it is usually assumed that both contributions are additive. In turn, these two transport channels are modeled with different dedicated codes. One of the key questions is whether this assumption is valid, or whether neoclassical and turbulent transports exhibit synergistic effects. We address this fundamental issue through the study of the transport of impurities, acting as passive scalars. Predicting impurity concentration is important for ITER, where tungsten particles coming from the divertor could lead to prohibitive radiative losses [1] and impact dramatically plasma performance and stability. Actually, on-axis accumulation of tungsten has been widely observed in tokamaks. While the very core impurity peaking is generally attributed to neoclassical effects [2], turbulent transport could well dominate in the gradient region [3]. We report here for the first time on self-consistent simulations of both transports by means of full-f and flux-driven gyrokinetic simulations, and present clear evidences of a neoclassical-turbulence synergy for impurity transport. It likely originates from the turbulence driven poloidal asymmetries, which depart from neoclassical expectations.

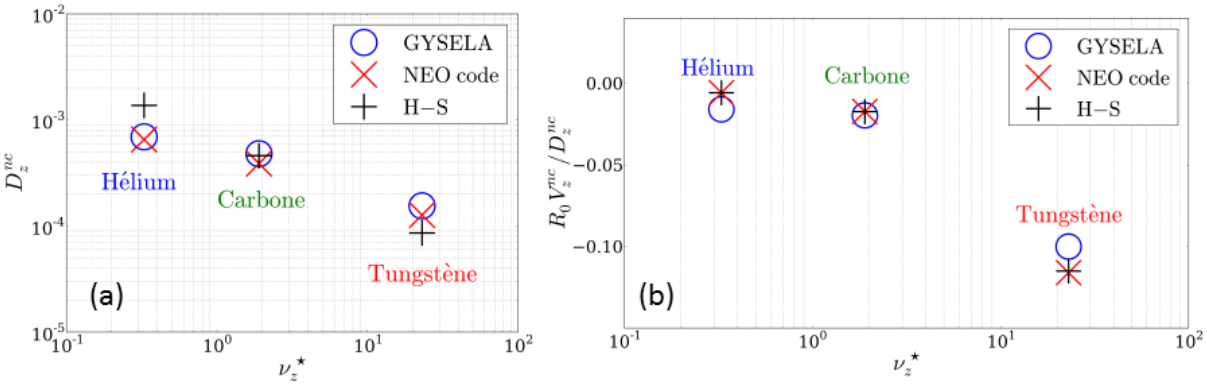

Figure 1: *Neoclassical (a) diffusion coefficient and (b) pinch velocity from GYSELA vs. the impurity collisionality* ν_{*z}. *Results from the NEO code [6] and theoretical predictions [7] are also plotted.*

The GYSELA code has been recently upgraded to evolve two ion distribution functions of arbitrary mass and charge (adiabatic electrons) [4]. The implemented multi-species collision operator, valid for trace thermal impurities, is successfully benchmarked [5]. It accounts for momentum and energy exchanges between species, and allows one to recover the main results of the neoclassical theory for impurity transport in all three collisionality regimes (banana, plateau, Pfirsch-Schlüter), especially the diffusion coefficient and the pinch velocity, Fig. 1.

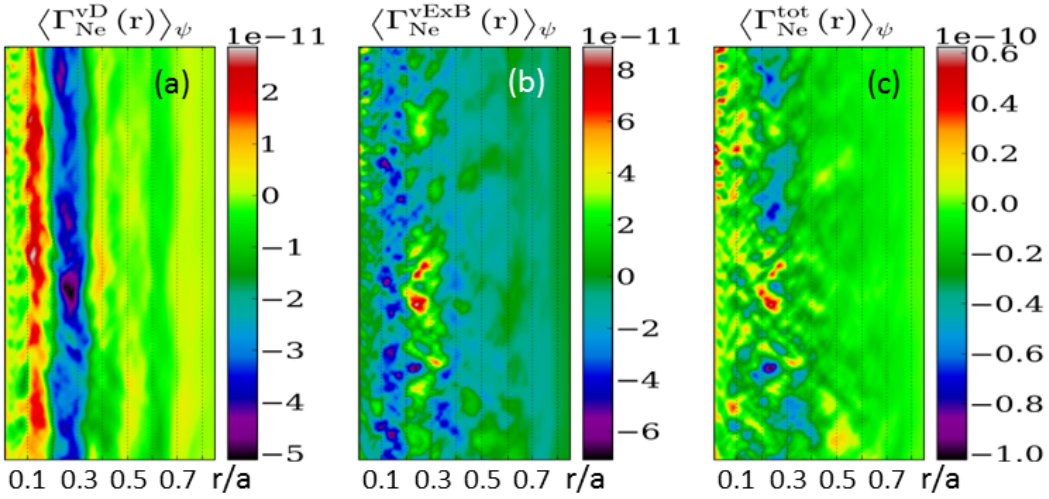

Figure 2: *Neon flux due to (a) the magnetic drift, (b) the electric drift and (c) total.*

For impurity transport studies, once the main ion species (deuterium) has reached the saturated regime, the simulations are restarted with an initial impurity density profile homothetic to the one of deuterium n_D, but at low concentration ($n_z/n_D \ll 1$). No particle source is added so far, and impurities remain at a trace level. Three impurities have been studied, helium, neon and tungsten. The collisionality of deuterium is chosen equal to $\nu_D^* = 0.1$ at the center of the simulation domain, so that the three collisionality regimes are covered (assuming equal temperatures, the collisionality of the various impurities scales like $\nu_z^* \approx \sqrt{2}\,(Z_z/Z_D)^2\,(A_D/A_z)^{1/2}\,\nu_D^* = 2\nu_D^* Z_z^2/A_z^{1/2}$). All simulations are performed at $\rho_{*D} = \rho_D/a = 1/150$. The number of grid points is the following: $(N_r, N_\theta, N_\varphi) = (256, 256, 32 \rightarrow 128)$, $N_{v_\parallel} = 128 \rightarrow 256$, and $N_\mu = 16 \rightarrow 32$. The total impurity flux is the sum of the magnetic and electric contributions:

$$\langle \Gamma_z^{tot} \rangle_{FS} = \left\langle \int d^3\mathbf{v}\, F_z\, (\mathbf{v}_{D,z} + \mathbf{v}_{E,z}) \cdot \nabla r \right\rangle_{FS} \tag{1}$$

Here, the magnetic $\mathbf{v}_{D,z}$ (low beta limit approximation) and electric $\mathbf{v}_{E,z}$ drifts are defined by:

$$\mathbf{v}_{D,z} = \frac{m_z v_{G\parallel}^2 + \mu_z B}{Z e B_\parallel^*} \frac{\mathbf{b} \times \nabla B}{B} \quad ; \quad \mathbf{v}_{E,z} = \frac{\mathbf{b} \times \nabla J_z.\phi}{B_\parallel^*} \tag{2}$$

with $\mathbf{b} = \mathbf{B}/B$ and J_z the gyro-average operator (see [4]). These two contributions are not fully equivalent to the neoclassical and turbulent components. Indeed, the neoclassical flux is the sum

of both magnetic drift and $E \times B$ axi-symmetric contributions (cf. [8, 9])

$$\left\langle \Gamma_z^{neo} \right\rangle_{FS} = \left\langle \int d^3\mathbf{v}\, F_z \left(\mathbf{v}_{D,z} + \mathbf{v}_{E,z}^{n=0} \right) \cdot \nabla r \right) \Big\rangle_{FS} \tag{3}$$

At medium Z (neon), both contributions are of the same order of magnitude. They tend to partially compensate, as already noticed for parallel momentum transport [10, 11], although exhibiting a rich dynamics (Fig. 2). The resulting average neon flux is inward for this set of parameters.

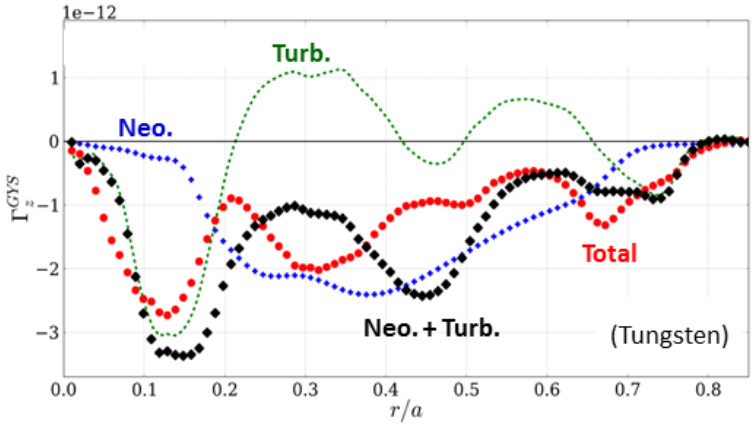

Figure 3: *Time-averaged tungsten flux in neoclassical, turbulent and full simulations.*

To look for possible synergies, three simulations have been performed for each impurity. (i) Purely neoclassic: all non-axisymmetric toroidal modes are filtered out at each time step (i.e. all Fourier modes with $n \neq 0$ are set to zero, with n the toroidal mode number). The neoclassical flux is the sum of electric and magnetic drift contributions. (ii) Mainly turbulent: single-species collisions only are retained (ν_{ii} and ν_{zz}), so that momentum or energy exchange between species is not taken into account. Retaining intra-species collisions is important and sufficient to account for the collisional damping of zonal flows, which efficiently contribute to turbulence saturation [12]. The turbulent flux is governed by the electric drift. (iii) Full: no simplification is made to the collision operator, nor any filtering applied to the electric potential. In the turbulent regime, the full collision operator is retained, involving intra- and inter-species collisions. In Fig. 3, the total tungsten flux (red) from the self-consistent full simulation is compared to the sum of the neoclassical and turbulent fluxes (black), coming from reduced simulations. This comparison is expected to provide the answer regarding the validity of current simulations where turbulent and neoclassical contributions are computed separately and simply added up. It appears that both fluxes differ from each other, by more than a factor 2 at some locations, showing that neoclassical and turbulent contributions are not additive [13]. One of the explanations likely comes from the existence of poloidal asymmetries which appear to be strongly modified –

reinforced magnitude and finer radial structure – in the presence of turbulence, as exemplified on Fig. 4. Indeed, these asymmetries are known to greatly change neoclassical coefficients, by one to two orders of magnitude [14, 15]. As a matter of fact, the number and the radial locations of the extrema of the fluxes for the purely neoclassical, mainly turbulent and full cases, Fig. 3, roughly coincide with those of the poloidal structures in Fig. 4(a-c), respectively.

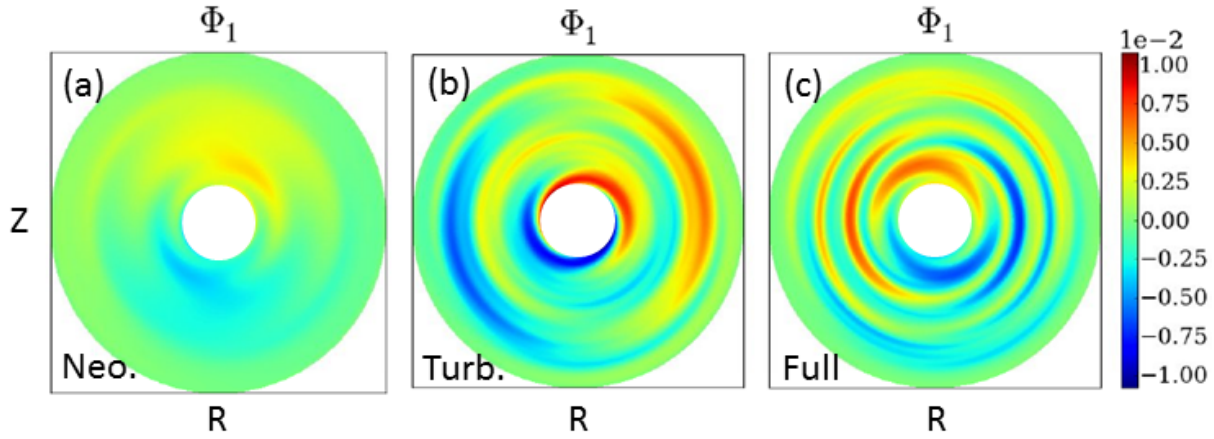

Figure 4: *Poloidal cross-sections of the* $(m,n) = (1,0)$ *component of the electric potential for the 3 simulations of Fig. 3.*

This evidence of synergy between neoclassical and turbulent transport of impurities is likely to have far reaching consequences when predicting tungsten concentration in ITER. Quantifying this synergy in various plasma regimes remains to be done, as well as finding routes towards a possible control of impurity transport.

References

[1] T. Pütterich et al., Nucl. Fusion **50**, 025012 (2010)
[2] F.J. Casson et al., Plasma Phys. Control. Fusion **57**, 014031 (2015)
[3] A. Loarte et al., Phys. Plasmas **22**, 056117 (2015)
[4] V. Grandgirard et al., to appear in Comput. Phys. Commun. (2015)
[5] D. Estève et al., Phys. Plasmas **22**, 122506 (2015)
[6] E. Belli and J. Candy, Plasma Phys. Control. Fusion **50**, 095010 (2008)
[7] S. Hirshman and D. Sigmar, Nucl. Fusion **21**, 1079 (1981)
[8] T. Vernay et al., Phys Plasmas **17**, 122301 (2010)
[9] P. Helander, Plasma Phys. Controlled Fusion **37**, 57 (1995)
[10] J. Abiteboul et al., Phys. Plasmas **18**, 082503 (2011)
[11] Y. Idomura, Phys. Plasmas **21**, 022517 (2014)
[12] P.H. Diamond et al., Plasma Phys. Control. Fusion **47**, R35 (2005)
[13] D. Estève et al., to be submitted to Nucl. Fusion (2016)
[14] T. Fülöp and P. Helander, Phys. Plasmas **6**, 3066 (1999)
[15] C. Angioni and P. Helander, Plasma Phys. Control. Fusion **56**, 124001 (2014)